A Cardiac Microtissue Platform With Integrated On-Chip Stiffness Measurement Capabilities

by

Christian Paniccia

A thesis submitted in conformity with the requirements for the degree of Masters of Applied Science

Department of Mechanical and Industrial Engineering
University of Toronto

A Cardiac Microtissue Platform with Integrated On-Chip Stiffness Measurement Capabilities

Christian Paniccia

Masters of Applied Science
Department of Mechanical and Industrial Engineering
University of Toronto
2021

Abstract

In vitro cardiac fibrosis models that monitor fibrotic markers have been developed to better understand fibrotic progression in humans. However, these platforms lack the ability to non-invasively monitor change in tissue stiffness, a hallmark of fibrosis. This motivated the development of a microtissue platform capable of non-invasive tissue stiffness measurement. Tissue stiffness on the platform was determined by force readouts through deflection of a PDMS rod and tissue strain achieved by noncontact magnetic stretching. As proof of concept, no difference was found in on-chip and tensile test measurements of rubber band stiffness. Tissue stiffness measurements on-chip failed due to reliability issues with the platform. However, when manually stretched, tissue stiffness determined on-chip was not different from that measured by atomic force microscopy. Full realization of this platform will result in fibrotic microtissue stiffness tracking throughout an experiment, leading to a better understanding of cardiac fibrosis progression.

Acknowledgements

I would like to thank my supervisor, Professor Craig Simmons, for the opportunity to work on this project. His guidance over the last 2 years has made me a better researcher, thinker, and learner. His patience with questions or concerns and overall mentorship throughout the project has made the last 2 years a tremendous experience.

I would like to thank Henrik, Alex, and Edwin for help with anything to do with fabrication and design. They always had the right answer. I would also like to thank Kayla and Omar from Prof. Sara Vasconcelos' lab for help and training with cell seeding protocols. Thank you Neda for all your help with AFM on such short notice. Thank you Zahra for being one of the kindest people I know, answering any question I had, and making the lab a brighter place. Thank you Mingyi, Alisa, and Jane, for coffee breaks during the day, and venting about any "grad school problems" we were experiencing. A big thanks to everyone in the Simmons Lab for making it one of the most welcoming environments I have had the pleasure to work in.

And thank you to my mom who has supported me in everything that I have done, for as long as I can remember, and my dad who would be proud of what I have accomplished the last couple of years.

Table of Contents

List of Tables

List of Figures

Chapter 1

1.0 Introduction

Heart failure is the end stage of many cardiovascular diseases (CVDs), where the heart is unable to pump blood at a rate that meets the metabolic requirements of tissue [1]. The inability of the heart to pump blood at the required rate is due to reduced ventricular compliance as a result of cardiac fibrosis [2]. After a traumatic heart event such as myocardial infarction, cardiac fibroblasts promote a healing response by synthesizing extracellular matrix proteins (ECM) which help maintain myocardial structural integrity. However, during a pathological response, ECM protein deposition is uncontrolled. The accumulation of matrix proteins leads to an increase in cardiac stiffness, which in turn reduces ventricular compliance, lowers cardiac output, and ultimately leads to heart failure.

While it is understood that cardiac fibroblasts play a key role in heart failure, knowledge of the progression of cardiac fibrosis in humans is lacking. To address this shortcoming, a number of groups have engineered cardiac tissue models which attempt to mimic the pathophysiological environment of fibrosis [3-10]. Through the use of human cells, incorporation of fibrotic causing agents, tracking of functional biomarkers in real time, and proof-of-concept drug responses, these fibrosis-on-a-chip models have been able to help us better study the complex pathways which govern the fibrotic response. The shortcoming of all these models however, is that they are not able to monitor change in tissue stiffness non-invasively throughout the course of their experiments. In a non-pathological environment myocardial stiffness is ~10 kPa, but as a result of fibrosis, can rise to nearly 40 kPa [11]. The increase in stiffness causes a positive feedback loop, activating quiescent cardiac fibroblasts, which results in continued collagen deposition, and a further increase in stiffness. The ability to monitor this change in stiffness in a physiologically relevant model would lead to a better understanding of the progression of fibrosis, potentially leading to enhanced drug screening and drug effect analysis.

This motivated the main objective of this thesis, which was to develop and fabricate a cardiac tissue platform which can non-invasively measure the stiffness of cardiac microtissues for potential future use in a physiologically relevant human cardiac fibrosis on-chip device.

1.1 The inflammatory response following myocardial infarction

Following a traumatic heart insult such as myocardial infarction, disruption to the extracellular matrix initiates an inflammatory and repair response. Myocardial infarctions cause rapid cardiomyocyte death, and due to the non-proliferative nature of cardiomyocytes, replacement of the structural integrity in the myocardium is taken up by extracellular matrix proteins. Cardiac fibroblasts secrete these proteins, such as collagen, which helps repair the heart after injury. The repair response is composed of three different phases, characterized by the different cytokines, chemokines, and proteins that play a role in producing a collagen-based scar to replace the dead cardiomyocytes.

The first phase of the response is the inflammatory phase. The intracellular contents released by cardiomyocytes following necrosis initiates this response by activating immune mechanisms such as activation of toll-like receptor mediated pathways, and generation of reactive oxygen species. Activation of these mechanisms activates nuclear factor–κB (NF-κB) which in turn begins to induce expression of key inflammatory cytokines and chemokines such as tumor necrosis factor α (TNF-α) and interleukin 1β (IL-1β) [12]. TNF-α and IL-1β promote matrix metalloproteinase (MMP) expression which leads to breakdown and degradation of the damaged extracellular matrix, ultimately paving the way for eventual scar formation [13]. Following the inflammatory response, the proliferative phase begins, marked by the inhibition of pro-inflammatory pathways and start of myofibroblast activation. At this point, cardiac fibroblasts begin to secrete fibronectin, which serves as a placeholder extracellular matrix. The secretion of fibronectin by cardiac fibroblasts is important during this phase as the presence of fibronectin causes differentiation of cardiac fibroblasts to myofibroblasts [14]. The maturation phase follows the proliferative phase. Myofibroblasts created during the

proliferative phase secrete extracellular matrix proteins such as collagen and begin to form scar tissue [2]. Formation of this scar helps maintain myocardial structural integrity in the absence of cardiomyocytes. The end of the maturation phase, and in turn the repair response, involves myofibroblast apoptosis [15].

1.2 Cardiac fibrosis

It can be seen then that cardiac fibroblasts play a key role in heart repair. Their ability to dispose extracellular matrix proteins such as collagen is crucial in scar formation and preventing rupture following myocardial infarction [16]. However, in a pathological cardiac fibrotic response, the collagen deposition by the cardiac fibroblasts becomes uncontrolled and fibroblast proliferation is increased. Increased deposition of collagen raises ventricular stiffness and can lead to impairment of systole and diastole function [17], while excess of cardiac fibroblasts can disrupt electrical conductions, leading to fatal arrhythmias [18]. While there are a number of factors that may cause a fibrotic reaction, uncontrolled differentiation of fibroblasts to the collagen secreting myofibroblasts is the primary culprit.

It was described in Chapter 1.1 how the presence of fibronectin during the proliferative phase of the repair response induces fibroblasts to differentiate into myofibroblasts. However, other factors, such as activation of certain molecular pathways and mechanical stress can cause myofibroblast differentiation and lead to a pathological fibrotic response.

One of the primary growth factors responsible for myofibroblast differentiation is transforming growth factor β (TGFβ). Prior to cardiac injuries, TGFβ is unable to react with its receptors. Following cardiac injury however, a number of molecules are released which activate TGF-β from its latent state and allow it to induce a fibrotic response. A similarity between these TGFβ activating molecules is their presence in the myocardium following injuries that damage the extracellular matrix [19]. Two key molecules capable of TGFβ activation include MMP2 and MMP9, two extracellular matrix degraders, whose activation of TGFβ helps strike a balance between matrix degradation and stability as

TGFβ has a role in preserving matrix integrity [19]. Activation of the renin-angiotensin-aldosterone system (RAAS) can also cause cardiac fibroblast proliferation and differentiation to myofibroblasts. During the repair process, macrophages entering the infarct site produce enzymes that activate angiotensin II. Angiotensin II causes the differentiation to myofibroblasts through the AT1 receptor interaction [20]. Endothelin (ET-1) is another factor that induces myofibroblast differentiation. It has been shown to increase cardiac fibroblast proliferation, promote collagen deposition, and create an apoptosis-resistant fibroblast [20].

Mechanical stress related activation of myofibroblasts is due to the mechanosensing nature of quiescent fibroblasts in cardiac tissue. In other organs, fibroblasts are shielded from strain by the extracellular matrix [21]. However, due to the cardiomyocyte's inability to proliferate following cardiac injury, fibroblasts in the heart must be ready to sense increased loads to respond with production of extracellular matrix proteins necessary for scar formation. Differentiation of fibroblasts to myofibroblasts due to increased mechanical load is a result of the increased focal adhesion of fibroblasts near sites of injury where they create stress fibers to remodel the tissue. The increased tension of the substrate has a synergistic effect with TGFβ to express alpha-smooth muscle actin (α-SMA),a hallmark of myofibroblast differentiation [22].

The presence cardiac fibrosis is related to a number of cardiovascular diseases. Excess of disposed collagen has a detrimental effect on the electro-mechanical function of the heart. Patients with heart failure stemming from diastolic or systolic dysfunction have shown significantly increased levels of myocardial fibrosis [23]. The increased stiffness of the myocardium from pathological collagen deposition lowers ventricular compliance. Diastolic function is impaired as the lowered compliance results in the ventricular chamber being unable to receive an adequate amount of blood during diastole [24]. Systolic function is impaired as the increased stiffness of the left ventricle walls reduces the ejection fraction of the heart. Heart failure eventually occurs from diastolic and systolic function as the overall cardiac output of the heart is reduced to a point where it cannot pump enough blood to meet the metabolic needs of tissues in the body [25].

Cardiac arrhythmia is another form of cardiovascular disease which could occur due to the cardiac fibrotic reaction. In a healthy heart cardiomyocytes send electrical signals between one another through connexins. Connexins are what allows current flow through the heart and propagate electrical impulses. Disruption to these pathways impairs the signal propagation, leading to irregular heartbeats. Cardiac fibrosis disrupts the excitation-contraction coupling between cardiomyocytes as connexins are impeded by the excess of collagen in the myocardium [26].

1.3 Motivation for physiologically relevant cardiac fibrosis models

Despite the knowledge of cardiac fibrosis molecular pathways and causes, understanding of fibrotic progression and fibrotic therapeutic effects in humans is limited. The use of animal models is one way in which the pathophysiology of heart failure and response to novel therapies can be discovered [27]. However, differences between human and animal physiology has made it difficult to extrapolate findings in animal models to predict responses in humans [28]. Approximately one-third of failed clinical trials are withdrawn due to cardiotoxicities not predicted by animal models [29], thus movement away from animal models for predictive effects of drugs and understanding of the complex pathways involved in cardiac fibrosis is necessary.

A number of two-dimensional models of cardiac fibrosis have been developed due to low cost, a higher throughput than animal models, and elimination of ethical concerns inherent with animal testing. In one example, *Zhao et al.* developed an *in vitro* cardiac fibrosis model capable of recapitulating a fibrotic response by patterning substrate rigidity to mimic a post-infarct myocardium [10]. The biomarker expression profile captured responses observed *in vivo* including elevated levels of α-SMA, fibronectin, and F-actin filaments on substrates with a higher stiffness. When an anti-fibrotic agent was applied to cells on the stiff substrates, the fibrotic biomarker profile was reduced, giving potential for the use of the platform for future pharmaceutical practices.

While two-dimensional models have their benefits compared to animal models, they suffer from the lack of physiological relevance related to cell-cell interactions, cell-ECM interactions, and tissue-specific function [30]. In the context of a cardiovascular system, *Pontes Soares et al.* demonstrated how the differences between 2D and 3D cardiac cell culture affected key aspects of the cells including overall morphology, contraction ability, presence of intercellular adhesion structures, and expression of cardiac differentiation markers [31]. Thus, to achieve the goal of mimicking the physiological and anatomical structure of the native heart environment to best study cardiac fibrosis pathophysiology and the effects of drugs, more complex 3D environments are necessary.

1.4 3D Cardiac fibrosis models

A number of 3D microenvironments to research cardiac fibrosis have been developed. The platforms, described in this section, were engineered to elucidate the pathophysiologies of fibrotic progression, including extracellular matrix remodeling, how electrophysiology and mechanical properties of the tissues change, and how models react to the application of antifibrotic therapies.

Spreeuwel et al. sought to develop an engineered microtissue platform that mimics cardiac fibrosis based on their analysis of established mouse disease models [6]. Their tissues were created with mouse neonatal cardiomyocytes and cardiac fibroblasts suspended in hydrogels with varying collagen percentage. Tissues were cultured around vertical PDMS posts which provided axial constraints for the tissues. Deflection of the PDMS posts when the tissues contract gave a contractile force readout. To mimic fibrosis in their tissues, either the collagen content or the number of fibroblasts were increased. By being able to tune these two parameters, they showed that an increase in cardiac fibroblast density hampered the contractile performance of their microtissues and disrupted the beating frequency, where as an increase in collagen content had little to no effect. Through development of this platform a better understanding of the microenvironment during fibrosis was discovered. While an increase in collagen content

is a biomarker of fibrosis, the increase in collagen itself does not seem to reduce the contractile force of the cardiomyocytes.

Spencer et al. aimed to uncover the complexities behind the role of cardiomyocyte-myofibroblast electronic interactions in the myocardium by measuring conduction velocity in engineering cardiac tissues [7]. In a fibrotic environment the presence of excess myofibroblasts impedes electrical conductions, which can cause arrhythmias**,** however, the details behind the electrophysiology are not well understood [8]. The engineered cardiac tissues in this study were created by isolating cardiomyocytes from 10-day old chicken embryos and suspending them in type I collagen. Fibrotic condition tissues were created by replacing 20% of the cardiomyocytes with myofibroblasts. Conduction velocity of the tissues was measured by mounting the tissues on electrodes and stimulating them. It was found that conduction velocity decreased with increased myofibroblast concentration. By engineering these 3D tissues with and without myofibroblasts, they concluded that myofibroblast structure and spatial organization plays a critical role in their contribution to fibrotic cardiac myopathy.

Sadeghi et al. looked to develop a platform that can capture the progression of fibrosis [9]. Unlike the previous two platforms that mimicked fibrosis with a pathological ratio of cardiac fibroblast/cardiomyocytes, they applied TGFβ1 to their cardiac tissues to induce a fibrotic reaction and observe its progression. By doing this, they aimed to produce an in vitro model that maintains cardiac fibroblasts in a quiescent state so the remodeling after the introduction of a pathological factor can be studied. Their tissues were fabricated from primary ventricular cardiomyocytes and cardiac fibroblasts isolated from neonatal Sprague Dawley rats and polymerized in GelMA hydrogels which matched the stiffness of native cardiac tissue. Application of TGFβ1 induced a fibrotic reaction in their tissues, marked by an increase in profibrotic genes such as type I collagen, fibronectin, and α-SMA. In addition, their disease model recapitulated functional properties of fibrotic cardiac tissue including asynchronous beating and higher stiffness.

These three studies demonstrated how to utilize three-dimensional engineered cardiac microtissues to uncover the complexities behind fibrosis pathogenesis. By mimicking a fibrotic environment through increased number of cardiac fibroblasts or application of TGF β1, a fibrotic signature could be achieved. This highlights the potential to use these platforms for disease models to study the efficacy of antifibrotic drugs. However, each of these system engineered their tissues using animal cells. Transition towards platforms utilizing human cells is needed to provide a human context as animal cells still fail to faithfully mimic human responses. Additionally, the platforms described lack the ability to longitudinally track a number of biomarkers of fibrosis throughout the duration of an experiment, relying on endpoint measurements such as immunostaining for relevant proteins and destructive stiffness measurements. The ability to measure functional properties of a tissue as it is undergoing a fibrotic reaction is tantamount to fully understanding the complexities involved in fibrosis pathogenesis.

Wang et al. engineered a human-cell based platform which recapitulates biomechanical and electrophysiological features of cardiac fibrosis, complete with noninvasive functional readouts such as active force, passive tension, and Ca^{2+} transients [5]. Cardiac tissues for this platform were generated using human induced pluripotent stem cell (hiPSC) derived ventricular cardiomyocytes mixed with cardiac fibroblasts. “Healthy” tissues were combined at a ratio of 3:1 cardiomyocyte:cardiac fibroblast, while fibrotic tissues were combined at a ratio of 1:3 cardiomyocyte:cardiac fibroblast. Tissues were suspended between two poly(octamethylene maleate (anhydride) citrate) (POMaC) wires. Deflection of these POMaC wires allowed continuous readouts of active force, passive tension, and Ca^{2+} transients.

Mastikhina et al. developed a human cardiac fibrosis on-chip model that activates a fibrotic reaction on chip through introduction of TGF-β [4]. Their model engineered cardiac microtissues using human cardiac fibroblasts mixed with human induced pluripotent stem cell-derived cardiomyocytes at a 1:3 fibroblast:cardiomyocyte ratio. With their tissues suspended around two PDMS rods as shown in Figure 1, they were able to assess contractile function in real-time as a noninvasive readout of fibrotic progression. Unlike

Wang et al.'s platform, they did not fabricate tissues with a pathological level of fibroblasts. Rather, by engineering tissues with a physiological level of cardiac fibroblasts, fibrosis progression due to a profibrotic cytokine was observed. The induction of fibrosis through TGF-β allowed the group to study the effects of antifibrotic drugs. When pirfenidone, an anti fibrotic drug used to treat pulmonary fibrosis, was administered, fibrotic tissues displayed lowered stiffness, passive tension, and cardiac fibrosis gene expression, while contractile force and collagen content remained constant. These findings matched those found in preclinical animal trials of pirfenidone, providing assurance that cardiac fibrosis on-chip platforms improve our understanding of cardiac fibrotic progression

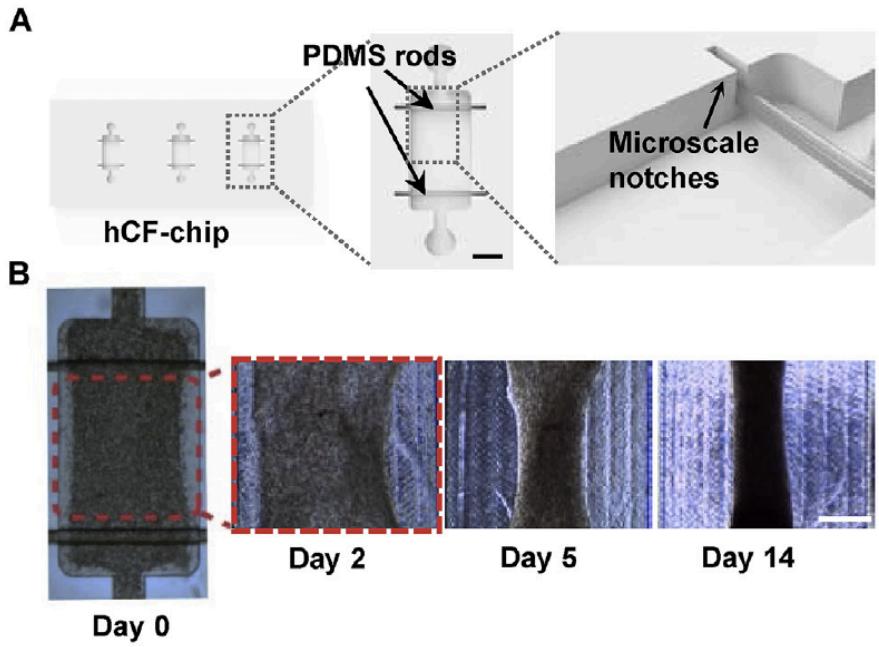

Figure 1- *Mastikhina et al.'s Human Cardiac Fibrosis on a Chip platform. A) Design of chip with two parallel horizontal PDMS rods for tissue seeding. Deflection of these rods at rest and during contraction enable non-invasive readout of passive and action tissue tension B) Cardiac microtissue seeded on platform, compacting over 14 days. Used with permission.*

These platforms are able to capture the complex physiological and pathological cues of a fibrotic myocardium through the use of human cells and relevant fibrotic causing factors. The platforms also provide proof-of-principle for using the platforms for analysis of antifibrotic drugs. In addition, the platforms allow for the longitudinal non-invasive monitoring of relevant functional fibrotic markers such as decrease in contractility and calcium transients. However, these platforms fail to monitor change in tissue stiffness,

one of the key biomarkers of fibrosis, non-invasively. Knowledge of tissue stiffness following a heart insult is crucial in determining when to apply certain anti-fibrotic therapeutics. Administering treatment too soon can halt the repair response and prevent fibroblasts from secreting enough collagen to maintain myocardial structural integrity after injury, while administering too late would result in the treatment having no effect at all [40].

1.5 Non-invasive tissue stiffness measurement platforms

The cardiac fibrosis platforms described in the previous section have shown the ability to mimic the fibrotic reaction. The limitation to the platforms however is that they rely on destructive endpoint measurements to measure one of the key biomarkers of fibrosis, tissue stiffness. Tissue stiffness is known to increase during the fibrotic response, and lack of monitoring the progression of tissue stiffness leaves an area of understanding to still be discovered. A number of microtissue platforms carry the ability to non-invasively measure the stiffness of tissue on-chip without destructive methods. Translation of a similar approach to a cardiac fibrosis on-chip platform would result in a platform which can non-invasively measure the stiffness of fibrotic tissue throughout the duration of an experiment.

Liu et al. sought to address the limitation of end-point analyses of tissue functional properties in bioreactors [33]. By developing a deformable membrane platform with integrated strain sensors that enabled mechanical stretching of 3D hydrogels they were able to measure hydrogel stiffness in situ. Hydrogels were chemically bonded to a deformable membrane with integrated strain sensors and through the use of a diaphragm pump, pressure was delivered through an inlet into the device, causing a deformation in the membranes. The membrane deflection was proportional to the bonded tissue's stiffness, thus by measuring the magnitude of the embedded sensor's resistive strain when a pressure was applied, tissue stiffness was able to be calculated.

Alhudaithy et al. aimed to develop a platform which can mechanically manipulate live microtissues with non-invasive stiffness monitoring, while at the same time being easily fabricated [34]. Their platform relies on the deformation of a PDMS membrane linked to an actuation arm controlled by an external actuator. This system controls the strain applied to the tissue by programming the actuation arm and when actuated, the attached sample undergoes tensile stretching.

The use of ultrasonic waves for non-destructive tissue stiffness measurements has also been explored. *Zareei et al.* developed one such platform to non-invasively measure the stiffness of ECM in real-time on a chip device [35]. By sending an ultrasonic wave between two piezoelectric transducers on either side of an agarose hydrogel with embedded fibroblasts, the stiffness of the hydrogel can be determined. The signal received by the transducer is dependent on the ultrasonic attenuation, which itself, is dependent of the stiffness of the hydrogel. Soft tissue would have a smaller attenuation, whereas stiffer tissue would have a higher attenuation.

Sidorov et al. developed a platform that applies a transverse force to the midspan of a cardiac tissue to determine the tissue stiffness [36]. On their platform stiffness was determined by moving a flexible probe into contact with a constrained tissue. The probe applied a transverse force when coming into contact with the midspan of the tissue, causing a deflection in the probe and tissue. Probe deflections were calibrated to certain forces, while the deflection of their tissue was recorded for use in their mathematical model. To determine stiffness from this approach, the tissue was modelled as a one-dimensional cable, an assumption that could be made if the tissues length was considered “long” compared to the diameter of the tissue. To make this assumption , the tissues were engineered with a ~10 mm length and diameter of ~ 400 μm. Using this method they measured a cardiac microtissue (composed of neonatal rat ventricular cells) stiffness of ~12 kPa, in the range of healthy myocardial tissue. The schematic of their platform is shown in Figure 2.

While these platforms have shown the ability to monitor tissue stiffness non-invasively, they are not adaptable for use in cardiac fibrosis on-chip platforms. Notably, they lack the ability to be adapted to measure mechanical markers such as contractile force or passive tension of tissues, or rely on engineering tissues too large for use on current devices. This motivates the need for a non-invasive stiffness measurement platform that is compatible with current human cardiac fibrosis on-chip devices. A combination of these technologies would be a milestone for studying the progression of fibrosis and its response to antifibrotic therapeutics.

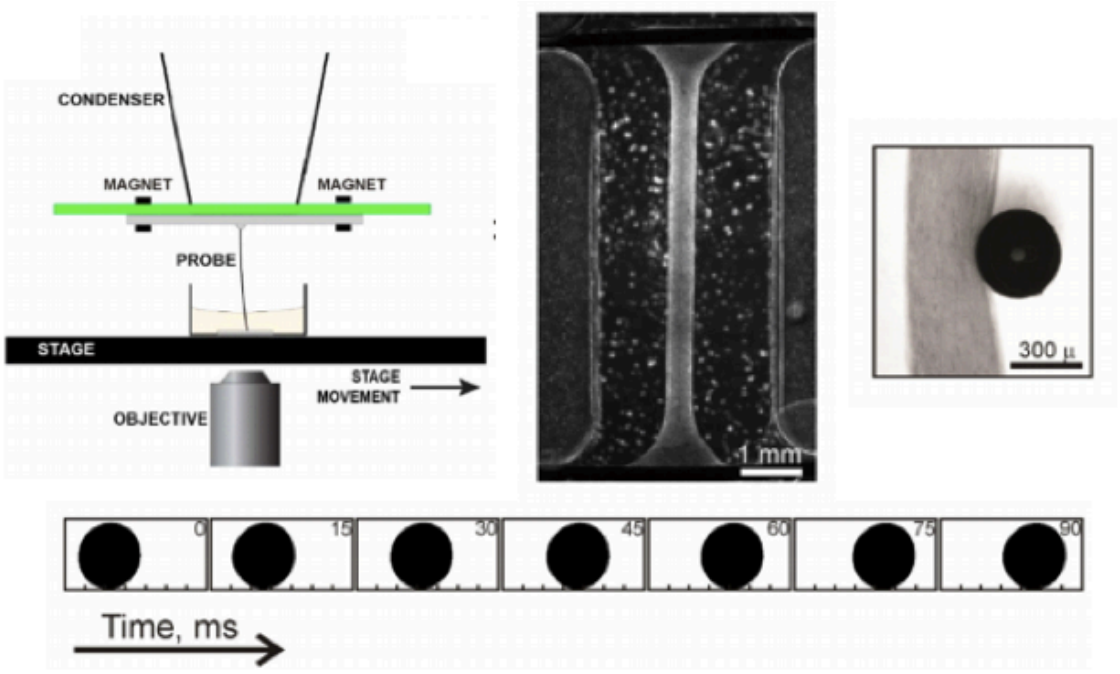

Figure 2 - Sidorov et al.'s I-Wire platform. A) Schematic of platform. Tissue platform is placed transverse to probe which is secured to microscope stage to allow for recording of tissue deflection when probed. B) Cardiac tissue on I-Wire platform. C) Probe deflecting cardiac tissue at midspan to measure tissue stiffness. D) Time lapse of position of probe during a cardiac tissue contraction. Used with permission.

Chapter 2

2.0 Rationale and objectives

2.0.1 Rationale

Understanding of cardiac fibrotic progression in humans is lacking, motivating the development of cardiac fibrosis on-chip platforms to study disease progression and drug response. The platforms incorporate three-dimensional human cell cardiac microtissues and are able to induce fibrosis through either pathological mechanical stimulation [3], introduction of TGF- β [4], or by culturing tissues with pathological fibroblast/cardiomyocyte ratios [5] . Further, the fibrotic phenotypes recapitulated on these platforms are responsive to administered anti-fibrotic drugs. However, to date fibrosis on-chip progression has been tracked through passive tension and contractile force, only two of the many pathophysiologies of fibrosis. Biomarker endpoint analysis and atomic force microscopy-based stiffness measurements at the end of experiments is currently the only other way to detect a fibrotic signature in these cardiac tissues. A method to non-invasively measure the stiffness of cardiac microtissues would allow for longitudinal monitoring of fibrosis progression on-chip, and help lead to a better understanding of the progression of the disease and a better understanding of drug effects.

2.0.2 Objectives

The overall goal of this thesis was to develop a cardiac microtissue platform which can non-invasively determine tissue stiffness. To this end, the following objectives were pursued:

Objective 1: Develop a platform that allows for non-invasive tissue stiffness measurement.

Experimental Approach: A two part system comprised of a tissue hosting chip and an actuation platform was constructed. The chip enables stiffness measurement through observation of a deformable PDMS rod. Tissue stiffness was measured by stretching the

tissue on-chip and observing the deflection of a PDMS rod attached to the tissue. The deformation of the PDMS rod was calibrated to a certain force. By observing the tissue deformation and knowing the force applied to the PDMS rod, the stiffness of the tissue was found using Hooke's Law.

Objective 2: Validate the platform by analyzing the difference between rubber band stiffness measurements made on-chip and in a tensile test.

Experimental Approach: Rubber bands were stretched on-chip and in a tensile test. Modulus values were compared between the two methods to determine if there was a difference in measured stiffness between methods.

Objective 3: Validate tissue stiffness measurements by analyzing the difference between cardiac microtissue stiffness measured on-chip and using AFM.

Experimental Approach: Microtissues were stretched on-chip and probed using AFM. Modulus values were compared between the two methods to determine if there is a difference between methods.

Chapter 3

3.0 Development of a cardiac microtissue platform with integrated on-chip stiffness measurement capability

3.1 Introduction

Cardiac fibroblasts are one of the key cell types in the heart due to their ability to secrete extracellular matrix proteins such as collagen [12]. The deposition of extracellular matrix proteins is a natural healing response which attempts to maintain myocardial structural integrity after heart traumas, such as myocardial infarction. However, in cases of pathological remodeling, the deposition of these proteins is uncontrolled, leading to a positive feedback loop of collagen accumulation in the extracellular matrix, which stiffens cardiac tissue, reduces ventricular compliance, and ultimately compromises the overall function of the heart [13].

The activation and progression of fibrosis in cardiac tissue is caused by numerous factors. In particular, tissue ischemia caused by myocardial infarction can result in fibrotic remodeling. Ischemia in the tissue sets off an inflammatory response which produces reactive oxygen species (ROS) which induce inflammatory responses. The ROS set off a multiprotein intracellular complex, called the inflammasome in cardiac fibroblasts, which results in the release of pro-inflammatory cytokines such as interleukin 1 beta (IL-1β) and tumor necrosis factor-α (TNF-α) and pro-fibrotic cytokines such as transforming growth factor-β (TGF-β) [12]. TGF-β is of particular interest as it is well documented that its secretion leads to the fibrogenic response through the differentiation of fibroblasts to myofibroblasts. The myofibroblast phenotype differs from fibroblasts as they express the contractile protein α-smooth muscle actin (α-SMA), promote collagen deposition, and secrete profibrotic factors which leads to additional recruitment of TGF-β, ultimately leading to the increase in stiffness of the myocardium and diastolic dysfunction [13][14].

Thus, targeting the TGF-β pathways represents a promising therapy for treating cardiac conditions associated with fibrosis. Studies conducted in animals have shown that anti-TGF-β neutralizing antibodies [37], synthetic peptides which interfere with TGF-β binding

[37], and inhibitors which block activin receptor-like kinase 5 (ALK-5) [38] attenuate TGF-β activity, and subsequent fibrosis in myocardial infarct and pressure overloaded rat models. However, difficulty in predicting drug reactions in humans from animal model data has arisen on multiple occasions [39].

To overcome this problem, a number of models for capturing human fibrosis-on-a-chip have been developed. *Mastikhina et al.'s* [4] human cardiac-fibrosis-on-a-chip included live force measurement of cardiomyocyte contraction and demonstrated fibrotic cardiac tissue response to anti-fibrotic drugs, but relied on atomic force microscopy, an end point analysis, to measure cardiac tissue stiffness, a key marker for progression of fibrosis. Similarly *Wang et al.'s* [5] Biowire model of interstitial and focal cardiac fibrosis was able to capture an accurate phenotype of fibrosis, yet relied on transferring their tissues to a Petri dish to measure their stiffness, and induced fibrosis through a non-physiologically relevant ratio of cardiac fibroblasts to cardiomyocytes in their gel constructs.

While these platforms for modelling cardiac fibrosis were able to successfully induce a fibrotic phenotype, they are unable to provide longitudinal measurement of one of the key biomarkers of fibrosis, stiffness, throughout the culture/treatment period. This limitation results in drug administration protocols being designed around set time points, e.g., administering fibrotic drug after 14 days, rather than protocols designed around precise degrees of fibrosis. This question of when to begin fibrosis treatment is debated. If antifibrotic treatment is begun too soon after an injury such as myocardial infarction, the heart tissue may rupture due to the production of the initial protective fibrotic layer being disrupted, while administering too late results in the fibrotic process being unaffected [40]. Thus, tracking a functional fibrotic marker such as tissue stiffness will allow drug administration protocols to be systematically studied and help elucidate the mechanisms that lead to pathological remodelling of the adult heart.

To address this unmet need, a cardiac microtissue platform with integrated, non-invasive stiffness measurement capabilities was developed. Through adaptation of *Mastikhina et al.'s.* existing cardiac-fibrosis on-chip design, a chip was designed and fabricated that

features a three-dimensional cardiac fibroblast tissue cultured around a horizontal PDMS rod and metal rod. A separate actuation platform comprised of a programmable stepper motor with attached neodymium magnet controls the translation of the metal rod through a magnetic coupling between the rod and the magnet. Linear displacement of the metal rod causes the tissue to stretch; by measuring the resulting deformation of the PDMS rod, one can calculate the tissue stiffness non-invasively using Hooke's Law.

3.2 Materials and methods

3.2.1 Chip and platform design and fabrication

A cardiac microtissue platform capable of non-invasively measuring the stiffness of cardiac tissue was designed and fabricated. The platform consists of a microchip that can host cardiac microtissues and an actuation platform comprised of a stepper motor with an attached neodymium magnet controlled by a programmable Arduino Uno. The actuation platform is able to accommodate a 35 mm Petri dish which allows the microchips containing cardiac microtissues to be cultured separately, and placed on the actuation platform when it is time to measure stiffness. An overview of the platform setup and chip is shown in Figure 3, with key parts labelled in Figure 3a and detailed in Table 3.

The microchip was designed to allow for cardiac tissue to be cultured around 2 parallel horizontal rods as shown in Figure 3b. The design includes a 1.5 mm x 3 mm x 500 µm rectangular chamber with a 200 µm slot and a 2 mm slot placed 3 mm apart to allow a polydimethylsiloxane (PDMS) rod and metal rod to be inserted, respectively.

The PDMS rods were fabricated using a 30:1 base to curing agent ratio, polymerized inside of a 27 gauge needle at 75 °C overnight. Once fully cured, the PDMS was pulled out of the needles, producing cylindrical rods with a ~200 µm diameter. The PDMS rods were cut in 2.5 mm increments, placed in the 200 µm slot, and fixed in place with small

drops of PDMS on the ends. The 100 μm diameter metal rods (McMaster-Carr # 8907K89) were cut in 2.5 mm increments.

Translation of the metal rod on the microchip is achieved using the actuation platform. The metal rod is magnetically coupled to the neodymium magnet affixed to the stepper motor when the Petri dish is placed on the platform. An Arduino Uno controls the stepper motor which allows the neodymium magnet to be displaced a prescribed distance.

The neodymium magnet chosen (McMaster-Carr #3360K384) was decided on due to its magnetic strength, polarity, and hole diameter. The magnetic strength, its maximum pull, of this neodymium magnet is 13 lbs. This strength was sufficient to couple to the metal rod through 2 mm of acrylic. Ceramic magnets tested with a maximum pull of 3 lbs did not produce a strong enough magnetic attraction to couple with the metal rod on chip and translate the rod when moved. A neodymium magnet magnetized through its diameter was chosen over a magnet magnetized through its thickness. This type of magnetization was chosen as it allows the metal rod to couple to a pole on the magnet and remain oriented perpendicular to the magnet path of movement as shown in Figure 4. A magnet with ¼ inch inner hole diameter was chosen to securely fit onto the stepper motor's lead screw.

The stepper motor chosen is a captive bipolar stepper motor (Haydn Kerk #28H41-2.1-915). This stepper motor was chosen as it had captive movement, a lead screw diameter compatible with magnet inner hole diameters on McMaster-Carr, and relevant step size precision. The captive movement of the stepper motor ensured that the lead screw would not rotate when in operation, thus keeping the magnet in a fixed position which is crucial for maintaining the correct polarity for metal bar orientation. The lead screw tip diameter of 0.225" allowed magnets with a 0.25" diameter inner hole to be secured with minimal adhesive. The step size of 25.4 μm was the smallest step size available and allowed for a level of precision in stretching tissues at physiologically relevant levels.

The stepper motor is controlled by an Arduino Uno microcontroller (Arduino cat#000073) with A4988 driver (UEETEK #10RZ652LJ22WFFMI0R6V). The code for the Arduino (Appendix A) was written to control the amount of stepper motor translation by indicating the number of steps (10 steps, ~250 μm), to ensure a slow translation speed (0.5 seconds, 1 step/0.05 seconds), to return the stepper motor to its original position by programming a clockwise and counter-clockwise rotation, and to hold the magnet in place for one second before returning to its original position. A 10 step (250 μm) translation of the stepper motor was used to generate approximately 8-10% strain in a ~3 mm cardiac microtissue. This strain is non-pathological and results in a measurable deflection in the PDMS rod. A step speed of 1 step/0.05 seconds was chosen in order to reliably maintain a magnetic coupling between the neodymium magnet and metal rod on chip, while still being greater than the lower limit pulse rate of the A4988 driver (1 step/0.1 seconds). A one second pause time between direction changes was chosen to give time to visualize the deflection in the PDMS on-chip.

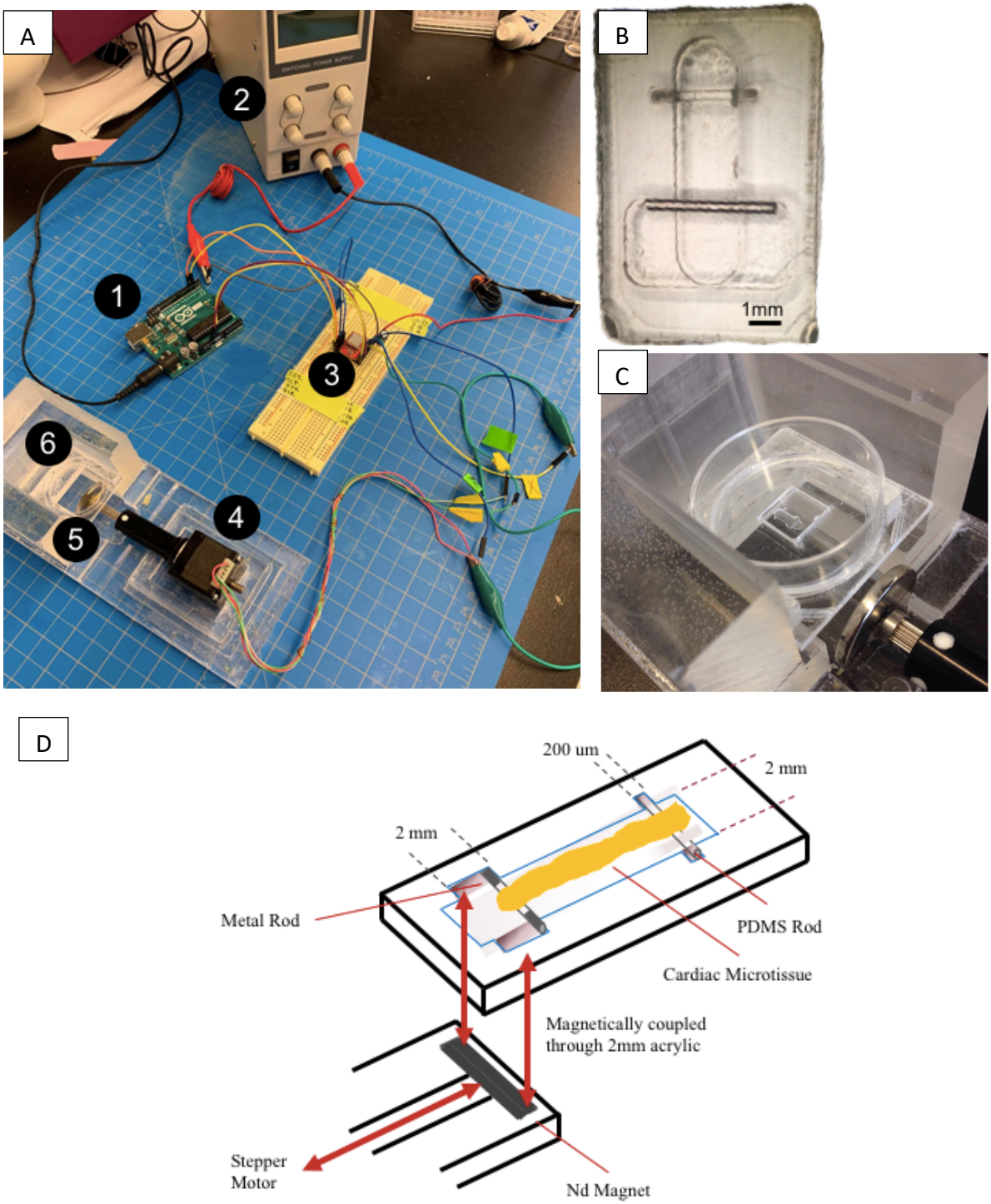

Figure 3 - A) Actuation platform set up with number labels for key parts detailed in Table 1. B) Microchip with fixed PDMS rod (top rod) and moveable metal rod (bottom rod). C) Microchip in 35 mm Petri dish on holder on actuation platform. Neodymium magnet attached to stepper motor below the Petri dish. D) Schematic of microchip and actuation platform setup.

#	Part	Notes
1	Arduino Uno (Arduino cat#A000073)	
2	Tekpower DC Power Supply (#TP6005E)	Runs at 12V, 0.2A to power stepper motor
3	UEETEK A4988 Driver (#10RZ652LJ22WFFMI0R6V	
4	Haydn-Kerk Bi-Polar Captive Stepper Motor (Haydn Kerk #28H41-2.1-915)	
5	Neodymium Magnet (McMaster-Carr #3360K384)	Diametrical magnetization
6	35 mm Petri Dish Holder	Laser cut from PMMA with exact fit for 35 mm Petri dish

Table 1 – Key parts in actuation platform setup

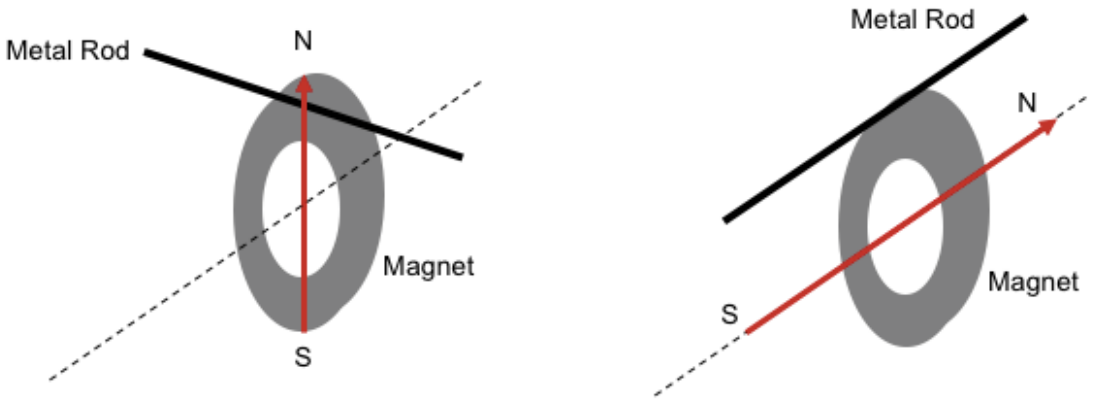

Figure 4 - Magnetization polarity of neodymium magnet determines the orientation of the metal rod on chip. A diametrically magnetized magnet (left) orients the metal rod perpendicular to path of magnet movement. A magnet magnetized through its thickness (right) orients the metal rod parallel to magnet line of movement.

3.2.2 Measuring elastic modulus on-chip

To measure the elastic modulus of tissue on-chip, assumptions about the platform and tissue must be made to utilize the equations in the mathematical model. The strains involved during the stretching process must be considered “small” and the tissue is assumed to behave as a linear elastic solid.

Small strains must be assumed in the model as when strains are large relative to the original material length, the change in overall material geometry due to the deformation can no longer be neglected, and a more rigorous definition of strains, stresses, and their rates with respect to original geometry must be used [41]. A deformation limit to assume small strains in the model can be determined by calculating the strain using the large strain-displacement relationship equation [42]

$$\varepsilon_x = \frac{\partial u}{\partial x} + \frac{1}{2}\left[\left(\frac{\partial u}{\partial x}\right)^2 + \left(\frac{\partial v}{\partial x}\right)^2\right] \quad (1)$$

where ε_x is the strain in the x-direction, $\frac{\partial u}{\partial x}$ is change in length in the x-direction normalized by original length in the x-direction, and $\frac{\partial v}{\partial x}$ is change in length in the y-direction normalized by original length in the y-direction. Thus, it can be seen that at small deformations, the squared values would become insignificant, and the strain in the x-direction, ε_x, would then be equal to the change in length in the x-direction normalized by the original length, $\frac{\partial u}{\partial x}$.

Figure 5 shows the resulting strain, ε_x, calculated using equation 1, assuming a certain change in length in the x-direction, $\frac{\partial u}{\partial x}$, and assuming a Poisson’s ration of 0.5, a fair estimate for most biologic tissues.

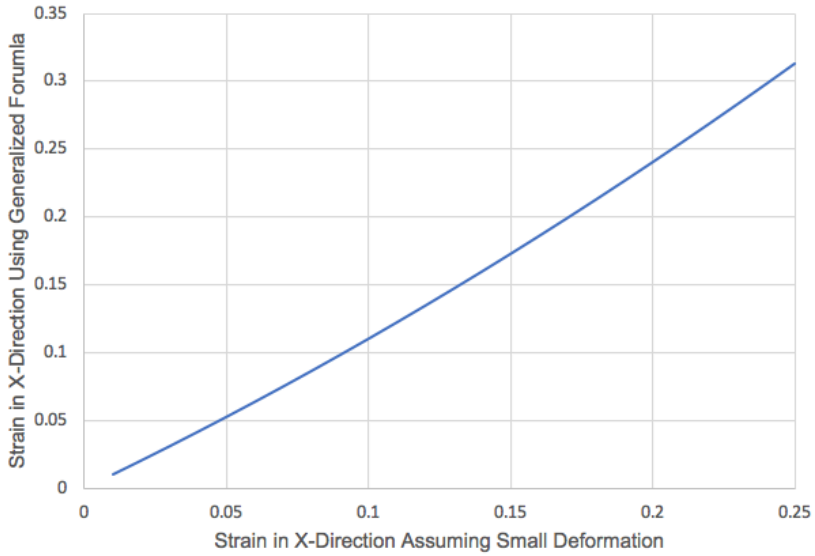

Figure 5 - Strain in material using generalized large-strain relationship equation vs. strain in material assuming small deformations

It can be seen that a change in length in the x-direction of 10% of the original x-direction length equals an 11% strain in the x-direction using the large-strain relationship equation. Thus, if the deformation applied to the tissue remains below 10% of its original length, small strains can be assumed, as strains resulting from changes in overall geometry would result in only up to 1% addition in strain and thus can be neglected for the purposes of this project.

The tissue also has to be assumed to behave as a linear elastic solid for the mathematical model to hold. Biomaterials are known to behave as viscoelastic materials. Viscoelastic materials exhibit both elastic and viscous characteristics when undergoing deformation, are dependent on strain rates, and experience creep and stress relaxation when stress and strain is applied.

In this project, the platform stretches the cardiac microtissue to a strain of 10%. If we assume that the strain applied to the tissue is a slow process and utilize the Voigt Model for viscoelastic materials, the material can be approximated as linear elastic.

The Voigt Model models viscoelastic materials as a spring and dashpot in parallel. When stressed, the strain in the spring must be equal to the strain in the dashpot. When solved, the model leads to the equation

$$\sigma = \varepsilon E + \eta \dot{\varepsilon} \quad (2)$$

where σ is the stress in the material, ε is the strain, E is the elastic modulus of the material, η is the viscosity, and $\dot{\varepsilon}$ is the strain rate.

Thus, from equation 2 it can be seen that a viscoelastic material under stress has an elastic response (εE), and a viscous response ($\eta \dot{\varepsilon}$). Furthermore, it can be seen that as the strain rate, $\dot{\varepsilon}$, approaches 0, i.e., a very slow deformation rate, the response to the material becomes strictly elastic.

Stroud et al. explored the viscoelastic properties of the myocardium [43]. At strain rates approaching 0 the stress-strain curve for the myocardium up to 10% strain was linear, indicating that any viscous damping was negligible. When the strain rate rose to 2.00 s^{-1}, the stress-strain curve became curvilinear, indicating that the viscous response in the myocardium could not be ignored and was behaving as a viscoelastic material. This is indicative of many biological tissues' stress-strain insensitivity to strain rate, where a 1000x increase in strain rate may result in only a two-fold change in stress [32]. Thus, with the stain rates applied throughout this study (~0.08 s^{-1}), the viscous response of the tissues can be assumed to be negligible.

With these assumptions, the tissue can be assumed to behave in a linear elastic manner and the elastic modulus of the tissue can be defined as

$$E = k * \frac{L}{A} \quad (3)$$

where E is the tissue's elastic modulus, k is the tissue's spring constant, L is the tissue's original tissue length, and A is the tissue's cross-sectional area at midspan.

The spring constant of the tissue was determined using Hooke's Law

$$F = k * \Delta L \quad (4)$$

where F is the force stretching the tissue and ΔL is the change in tissue length.

The change in length of the tissue was determined by programming the stepper motor to displace the metal rod a prescribed amount (Δd) and imaging the resulting deflection of the PDMS rod (δ) caused by the change in length of the tissue (Figure 6). The change in length of the tissue is then

$$\Delta L = \Delta d - \delta \quad (5)$$

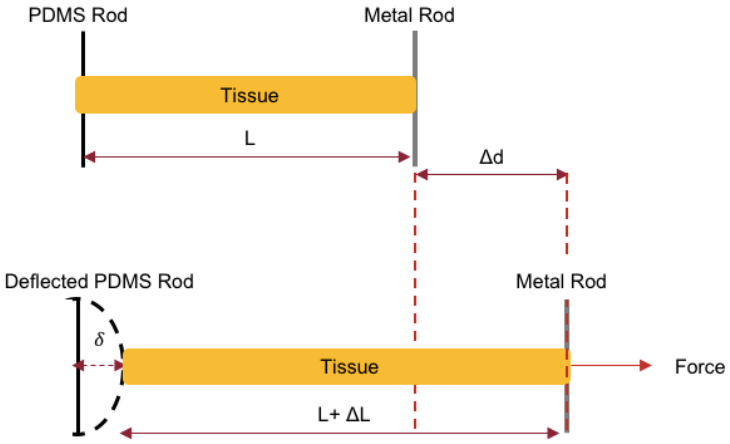

Figure 6 - Representative diagram of a force displacing the metal rod (Δd) causing a change in tissue length (ΔL) and deflection in the PDMS rod (δ).

The force stretching the tissue is equal to the force causing a deflection in the PDMS rod and is determined using a force-deflection calibration curve. The calibration curve for the PDMS rods was constructed by applying an increasing amount of suspended weights to the midspan of the PDMS rod and imaging its deflection at each respective weight.

Thus, to find the stiffness of the tissue, the deflection of the PDMS rod is imaged. From the deflection in the PDMS rod, a corresponding force stretching the tissue is found from the force-deflection calibration curve. The stiffness of the tissue is then found using Hooke's Law and the corresponding force and change in tissue length. Finally, once the stiffness of the tissue is determined, it is normalized by the tissue's geometry to determine the tissue's modulus.

3.2.3 Initial validation of stiffness measurement on-chip

To validate the elastic moduli measurements made on-chip, rubber bands with moduli similar to myocardial tissue (8-10 kPa) were tested both on-chip and in a tensile tester and their moduli were compared to test for differences between the two methods. To determine the elastic modulus of the rubber bands on chip, 1 cm long rubber bands were tied around the midpoint of the fixed PDMS rod and the metal rod. The metal rod was displaced 5 mm by the stepper motor and the resulting deflection in the PDMS rod was imaged (Figure 7). The deflection in the PDMS rod was matched with the corresponding force in the force-deflection calibration curve for 5 mm long, 30:1 ratio PDMS, with a rubber band at midspan (Figure 8). The change in length of the rubber band was determined as the difference between the metal rod displacement and PDMS rod deflection as in Equation 5. The stiffness of the rubber band was then found using Hooke's law with the force from the calibration curve and the change in length of the rubber band, as in Equation 3. Finally, the stiffness value of the rubber band was normalized by the rubber band's cross-sectional area, approximated as a circle: $A = \pi * r^2$, with the radius of the rubber band being 20 μm, and elastic's length, as in Equation 3.

The same rubber bands were then tested in a tensile tester (Test Resources 840 – 1 N load cell) to test the hypothesis that there is no moduli difference compared to rubber bands measured between the two methods.. The rubber bands were placed in the tester grips with 1 cm spacing and stretched at a rate of 1 mm/second to a final length of 1.5 cm. The modulus was calculated by fitting the linear portion of the stress-strain curve.

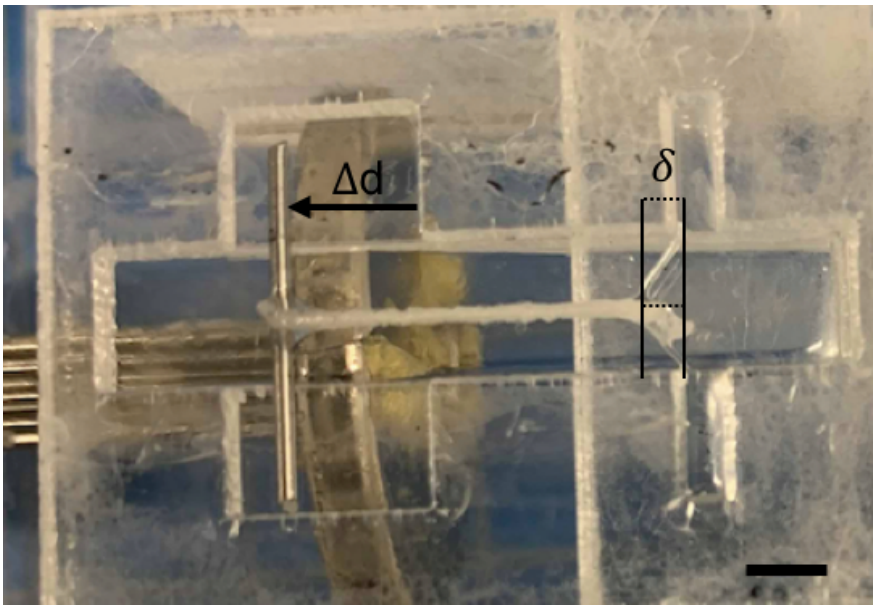

Figure 7 - Rubber band stretched on-chip by displaced metal rod causing deflection in PDMS rod. Scale bar = 1 mm.

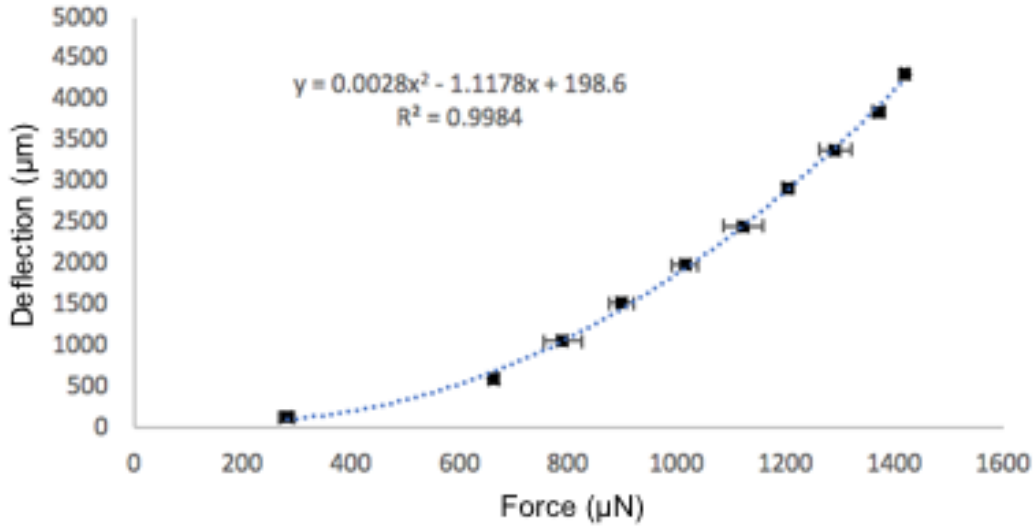

Figure 8 - Force-Deflection calibration curve for 5 mm PDMS rod (30:1 base:curing agent) with weights suspended from rubber band tied at midspan.

3.2.4 Cell seeding on-chip

To produce 3D tissues on-chip, the chips were first prepped by washing with 70% ethanol for ten minutes followed by rinsing with sterile PBS for ten minutes. After washing, chips

were coated with 5% weight/volume bovine serum albumin (BSA) solution (Sigma cat#A9418) by submerging the chips in the BSA solution for 15 minutes. After 15 minutes, the BSA solution was aspirated and the chips were allowed to dry for 45 minutes before cells were seeded.

Human ventricular cardiac fibroblasts (Lonza cat# CC-2904) were cultured in T175 flasks with DMEM (Gibco) supplemented with 20% fetal bovine serum (FBS) (Gibco) and 1% penicillin/streptomycin (Gibco cat#15140112). Fibroblasts between passages 4-8 were used for experiments.

Cells were seeded in fibrin gels composed of Matrigel (Corning cat# 356234– 9 mg/mL batch concentration) (1 mg/mL final concentration in fibrin solution), fibrinogen (Sigma cat# F4883)(5 mg/mL), aprotinin (Sigma cat# A1153)(0.00825 mg/mL), and DMEM. ~120,000 Cells were added to fibrin gel solution before seeding. 48 U/mL thrombin (Sigma cat#SRP6557-250U) was added to solution immediately before seeding. 8 µL of fibrin gel solution was pipetted onto chip. Chips were placed in an incubator for 45 minutes to allow gels to polymerize before adding media.

3.2.5 Measuring modulus of tissue on-chip

After 14 days on-chip, measurements of the cardiac fibroblast tissues' modulus were attempted using the actuation platform. The 35 mm Petri dish with the chip was aligned on the platform's holder with the metal bar end of the chip over the neodymium magnet. The metal bar was displaced 0.3 mm through the stepper motor movement. The intent was to hold the tissue in position to record the deflection of the PDMS rod and dimensions of the tissue and then return the metal bar to its original position. However, this method to did not work, as the tissues were unable to be stretched without damaging the tissues due to weak tissue adherence to the metal rod and sensitivity of the platform. These issues are explained in greater detail in Section 4.0. To circumvent these limitations but still demonstrate the principle of the platform, measurements were made as planned but by displacing the metal bar manually by ~0.3 mm using tweezers while taking video to

measure the metal bar displacement, PDMS rod deflection, and tissue dimensions. Deflection of the PDMS rod allowed force to be determined through the force-deflection calibration curve ($F = 1.55x + 0.00256x^2 + 0.002156xy$) in *Mastikhina et al.* where F is the force in the tissue, x is the deflection of the PDMS rod, and y is the width of the tissue attached to the rod [4]. This curve was used as it accounted for variable tissue width at the rod and was constructed using the same PDMS curing density and length as our study.

To confirm the elastic modulus measurements made on-chip, the tissues tested on the chip were also tested off-chip. Elastic modulus measurements were made by nanoindentation using atomic force microscopy (AFM). A JPK atomic force microscope (AFM; Bruker JPK NanoWizard 4 XP: High Resolution, Large Format Bio-AFM, Cambridge, United Kingdom) was used to determine the stiffness of the engineered tissues at the endpoint. Tissues were taken out of the device keeping the PDMS and metal rods attached and secured in place on top of charge adhesive glass slides by using cover slips to hold the rods down. PBS was added to keep the tissue hydrated. The indentation tests were conducted using force spectroscopy contact mode. Tip-less silicon nitride AFM cantilevers (Bruker, MLCT-O10, cantilever D with a nominal spring constant of 0.03 N/m) were functionalized using 10 μm radius spherical polystyrene beads. The precise spring constants were calibrated using the contact-based thermal tune method. Five locations were probed near the center of the tissue. Each of these locations was composed of a 10 μm × 10 μm area in which five independent points were indented. The indentation tests were repeated five times at every single indentation point, i.e., five technical replicates per point. Indentation force-deflection curves were recorded, and the stiffness was obtained from the extend curves using the Hertz/Sneddon model. Data analysis was performed using the JPK Data Processing software (version 6.3.11). Further AFM indentation tests were conducted at 10 locations along the length of the engineered tissue, following the same procedure explained above. Five stiffness values were obtained for every single indentation point. The values were then averaged, and the mean value was considered as a stiffness data point. Statistical analysis was performed using GraphPad PRISM (version 5.03).

3.3 Results

3.3.1 Platform's measurement of elastic stiffness compared to tensile test

To validate the stiffness measurements made on-chip, six rubber band samples stretched on-chip were stretched in a tensile tester. On-chip stiffness measurements (10.80 ± 1.53 kPa) were within 3% of tensile test stiffness (11.14 ± 1.33 kPa). A Student's paired t-test confirmed there is no significant difference (p=0.5) between measurements made on-chip and measurements made using the tensile tester.

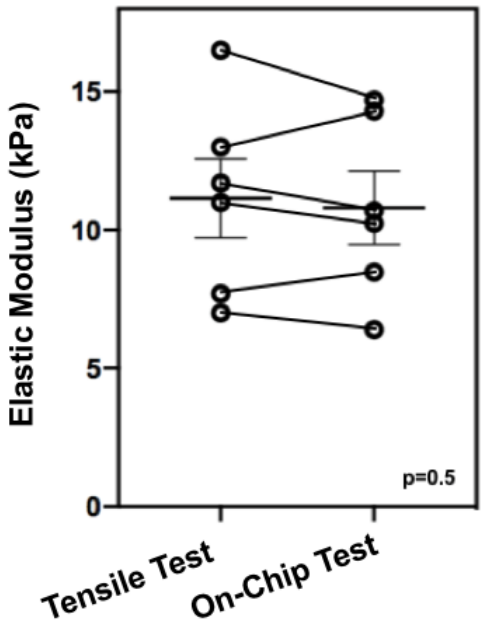

Figure 9 - Elastic moduli of rubber bands measured using tensile test and on-chip. (Student's paired t-test. S.D. p=0.5.).

3.3.2 Tissue stiffness measurements on-chip

Tissue stiffness measurements made on-chip were validated by comparing to AFM stiffness measurements. Five cardiac microtissues were stretched on-chip by translating the metal rod ~300 μm manually using tweezers as shown in Figure 10. Tissues were selected if they displayed no evidence of tearing when being stretched. The same five cardiac microtissues were affixed to glass slides and probed using AFM. The stiffness of the cardiac microtissues measured on-chip (1.148 ± 0.21 kPa) did not differ significantly

to the stiffness measurements found using AFM (1.042 ± 0.28 kPa), as shown in Figure 11.

Tissue stiffness measurements using AFM were also made along the length of the tissue (PDMS rod end to metal rod end) to determine heterogeneity of the tissue and if local stiffness differs depending on proximity to the PDMS rod or the metal rod. Three tissues were probed along their length using AFM with resulting moduli shown in Figure 12. One-way ANOVA was performed on each of the separate tissues' modulus data. Each of the tissues accepted the null-hypothesis ($p>0.05$) for Bartlett's test, indicating homogeneity of the variances in the probed locations' data, thus allowing use of ANOVA to analyze the variance amongst the probed locations. A post-hoc Dunnet's test was performed between the average modulus of the tissue (data used in Figure 11) and each location probed along the length of the tissue. All tissues displayed a statistically significant variance ($p<0.0001$, $p<0.0001$, $p=0.013$) in modulus amongst the locations probed. Dunnet's test comparisons for each tissue demonstrated heterogeneity along the tissue length, but without a clear pattern of one region consistently being stiffer than another across the three tissues.

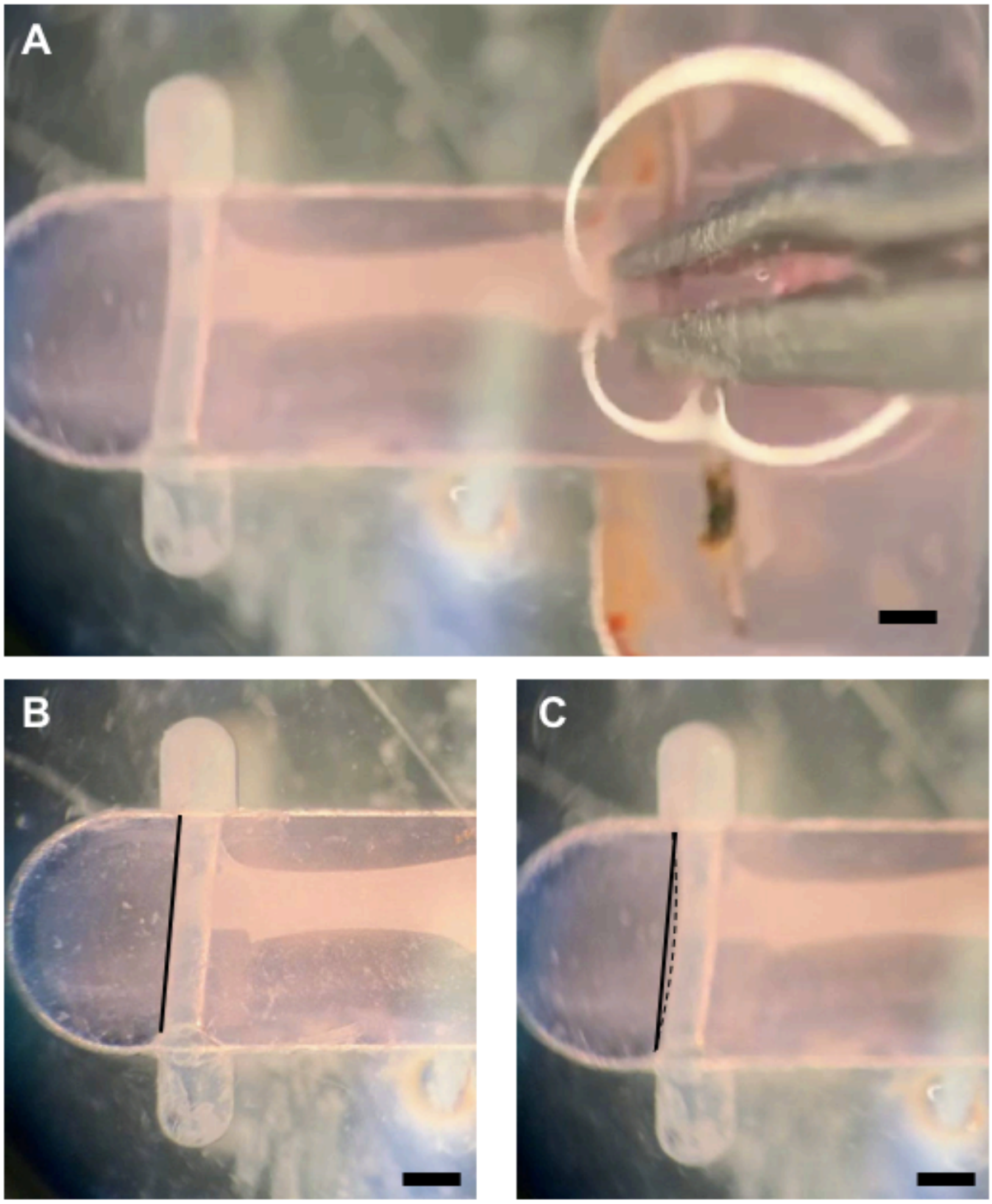

Figure 10 - Deformation of PDMS rod through displacement of metal rod using tweezers. A) Full view of chip. Metal rod is displaced and PDMS rod is deflected. B) PDMS rod before metal rod displacement. Black line shows original position of PDMS rod edge. C) PDMS rod after metal deflection. Solid black line is original position of PDMS rod edge. Dashed line is edge is PDMS rod when metal rod is displaced, visualizing the deflection of the rod. Scale bar = 200 μm.

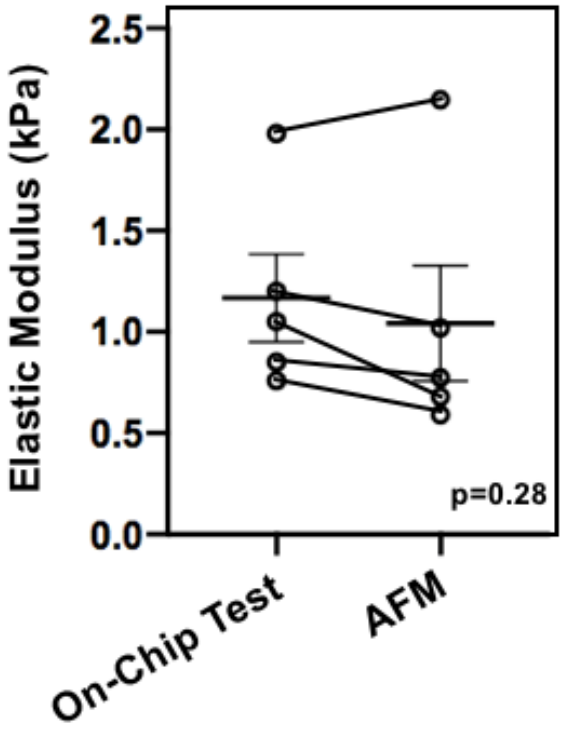

Figure 11 - Elastic moduli *of cardiac tissues measured on-chip and using AFM*. (Student's paired t-test, S.D. p=0.28)

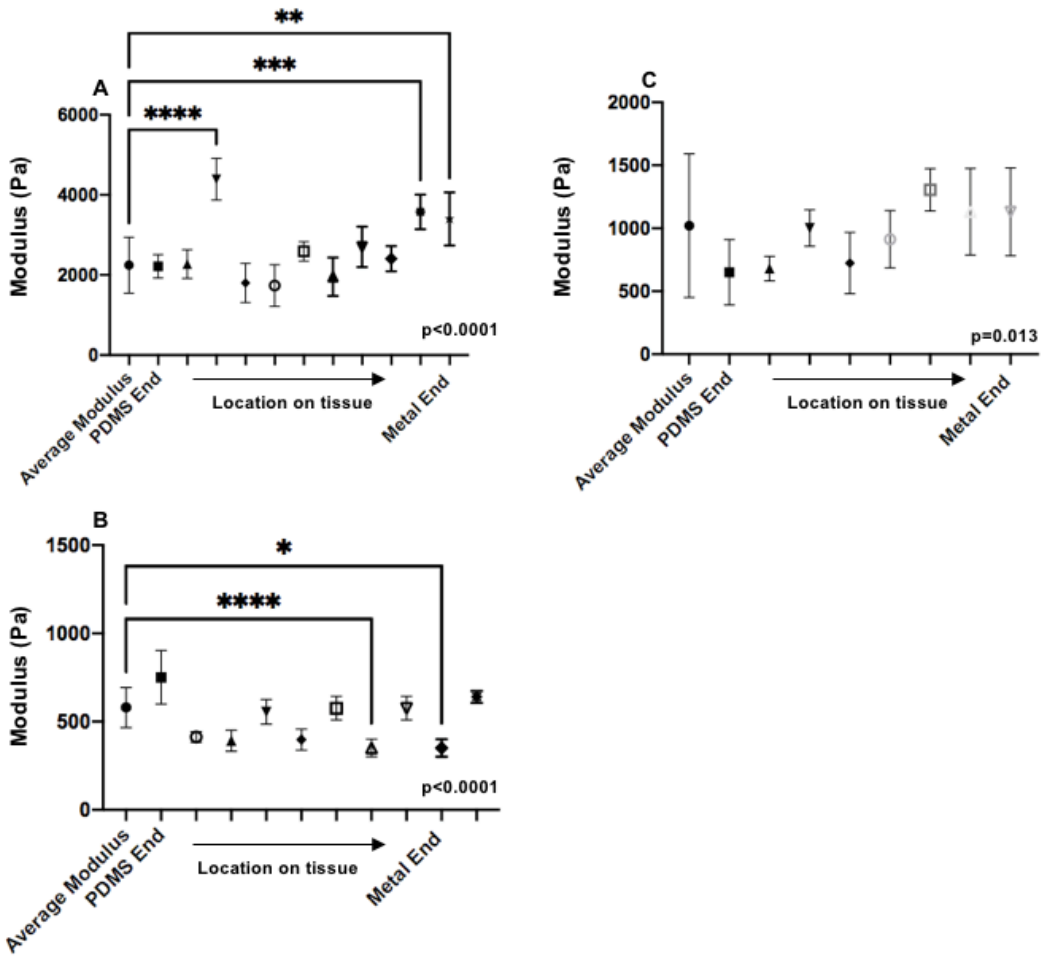

Figure 12 - Stiffness values of locations probed along the length of a tissue from PDMS rod end to metal rod end. Location of probe on tissue indicated by arrow on graph showing location relative to PDMS rod or metal rod end. Average modulus value shown on each graph is stiffness measurement of random probe location on tissue. A) Variance of moduli amongst probed locations differ significantly ($p<0.0001$). Three locations differ significantly compared to average modulus. **** = $p<0.0001$, ***= $p<0.001$, **=$p<0.01$. B) Variance of moduli amongst probed locations differ significantly ($p<0.0001$). Two locations differ significantly compared to average modulus. **** = $p<0.0001$, *=$p<0.5$. C) Variance of moduli amongst probed locations differ significantly ($p=0.013$).

Chapter 4

4.0 Discussion and Future Work

In this study, a platform was developed for the purpose of non-invasively measuring the stiffness of cardiac microtissues, which is essential in monitoring the progression of diseases such as cardiac fibrosis. The platform was constructed as a two part system consisting of a microchip where the tissue is hosted and a separate actuation platform where the chip can be placed at time of testing. A cardiac microtissue is cultured around a fixed PDMS rod and a moveable metal rod on-chip, and the stiffness is determined by displacing the metal rod and imaging the resulting deflection in the fixed PDMS rod as the tissue is stretched. The metal rod is non-invasively displaced when the chip is placed on the actuation platform and couples to a neodymium magnet attached to a stepper motor. The stepper motor can then translate the magnet a prescribed distance through a program on an Arduino Uno. This would allow the stiffness of a cardiac microtissue to be tested throughout the duration of an experiment, and not be limited to an endpoint stiffness analysis as in other cardiac fibrosis on-chip devices [3-5].

The platform was validated by comparing the measured moduli of rubber bands on-chip and in a tensile tester, with no statistically significant difference detected. Microtissues composed of cardiac fibroblasts polymerized in fibrin gels were stretched on-chip to determine their moduli and subsequently probed using AFM to confirm the stiffness measurements made on-chip. While using the actuation platform to stretch the tissues was unsuccessful due to reliability issues, the tissues were able to be manually stretched on-chip, and imaged to determine their moduli. Moduli values of the tissues measured on-chip did not differ from stiffness measurements made using AFM, giving preliminary validation of the platform.

4.1 Heterogeneity of AFM stiffness measurements

The similarity in measured modulus values of elastic bands gives promise that the platform is able to measure the stiffness of a material non-invasively. However, it is

important to note that when comparing the on-chip tissue measurements to AFM measurements, that AFM probes a 10 μm x 10 μm area and resembles a local stiffness measurement, which may not be representative of the tissue as a whole. To determine if there was local stiffness heterogeneity, AFM measurements were taken along the length of three cardiac tissues, from the metal rod end to the PDMS rod end. It was found that all of the cardiac tissues displayed stiffness heterogeneity when analyzed using ANOVA, but without a clear pattern of one region being consistently different than others across the three tissues. All tissues displaying heterogeneity motivates the need to perform off-chip validation tests with a method that measures the bulk stiffness of the tissues. This becomes a crucial next step for validating the platform modulus measurements of fibrotic tissues. *Mastikhina et al.* observed a high degree of heterogeneity in their fibrotic tissues when measured using AFM, with a 0.6-9.2 kPa range of stiffness [4]. The CellScale Microsquisher is one piece of equipment that can perform a bulk tensile test measurement on the tissues similar to the type of stiffness measurement performed on-chip, and could potentially serve as a better form of tissue stiffness measurement validation.

The modulus of the tissue at the metal rod end differed from the local average stiffness of the tissue on only one of the three tissues tested. Therefore, it is unlikely that the rigidity of the metal rod is promoting local cardiac fibroblast differentiation to myofibroblasts as seen in stiff plastic Petri dish cultures [45]. However, this was a sample size of only three tissues and further investigation is needed. Along with AFM measurements, staining for α-SMA, a biomarker of myofibroblasts, could help determine if the rigidity of the metal rod is having an effect on fibroblast differentiation in that local area.

4.2 Modulus differences between different platforms

The moduli of the cardiac tissues measured on-chip and by using AFM were 1.148 ± 0.21 kPa and 1.042 ± 0.28 kPa, respectively. It is difficult to draw comparisons between the modulus values found on-chip to other modulus measurements of human cell cardiac microtissue models as the density of cells and cell composition differed from other studies. However, some insights can be inferred.

Wang et al. measured a modulus of ~8 kPa in control tissues using the CellScale Microsquisher stretching test. This is nearly 8x stiffer than the on-chip modulus measurements from our study. However, *Wang et al.* engineered tissues of ~55 x 10^6 cells/ml at a ratio of 3:1 cardiomyocyte:fibroblast and conditioned their tissues using electrical stimulation for 7 weeks. The process of electrical conditioning was to induce a mature phenotype in the cells, marked by increased active force. Their modulus measurement of 8 kPa is comparable to native myocardium, and thus might be resembling a more physiologically relevant cell make up than our tissues composed of strictly fibroblasts.

When comparing to *Mastikhina et al.'s* study, modulus values were similar. AFM measurements were compared as that was the common method used in both studies. Their measurements of non-fibrotic tissue moduli were in the range of 0.6-3.6 kPa. Our measured AFM modulus of 1.042 kPa fits in this range, however the question of comparing between studies of different cell densities still must be asked. *Mastikhina et al.* engineered non-fibrotic tissues of 20 x 10^6 cells/ml at a ratio of 3:1 cardiomyocyte:fibroblast. This is twice the cell density of our tissues (~10 x 10^6 cells/ml). However, comparisons between AFM could possibly be less sensitive to overall cell density as it is a surface measurement. The same fibrin gel recipe was used in both studies as well, which supports the idea that the makeup of the local surfaces probed using AFM were similar in each of our studies, resulting in similar modulus measurements.

Our tissues did not compare to the stiffness of native myocardial tissue (~8 kPa). This was not expected as our tissues, composed of 100% cardiac fibroblasts, do not match the physiological makeup of the native myocardium. Future work would involve engineering microtissues with cardiomyocytes to better recapitulate the myocardium cellular makeup.

4.3 Comparison to other non-invasive stiffness measurement platforms

The main advantage the platform designed in this study has over other non-invasive tissue stiffness measurement platforms is the ability to be easily integrated into current cardiac fibrosis on-chip platforms. The platform's chip design is a slight modification of the type of chips used in *Mastikhina et al.'s* and *Wang et al.'s* platform. Tissues are seeded around 2 horizontal rods, with the difference in our design being that one of the rods is a free-to-move metal rod and can be displaced to stretch the tissue and measure its modulus. If the metal rod is in its original position, contractile force monitoring can still be performed by the deflection of the fixed PDMS on our chip. Bulging membrane platforms such as *Liu et al.'s* do not possess the capability of real-time readouts of active tension and passive force.

Our platform applies a uniaxial strain to the tissue to measure the stiffness. As a result, the strain profiles in the tissue are expected to be uniform throughout. This carries both advantages and disadvantages compared to systems which provide a three-dimensional deformation to tissues, resulting in a non-uniform strain profile. *Liu et al.'s* bulging membrane platform was shown to provide this type of non-uniform strain distribution. When pressure was applied to deform the membrane, strains could vary from 20% at the top of the membrane to 1% near the outer edges [46]. This type of heterogenous strain distribution more closely resembles the physiological strains experiences by biological tissues, such as the myocardium. For example, modelling the left ventricle as a isotropic sphere as opposed to an anisotropic ellipsoidal geometry has resulted in a 50% error in measuring wall stress [47]. However, a uniform strain results in a more accurate bulk tissue stiffness measurement. Ultimately, the goal for this thesis was to be able to measure tissue stiffness non-invasively. Thus, priority was given to engineering a platform to most accurately measure stiffness.

Sidorov et al.'s I-Wire platform is a cardiac tissue platform capable of monitoring mechanical characteristics such as active tension non-invasively as well as tissue stiffness. However, the main assumption made in their study was that their tissue is modelled as a one-dimensional cable. For this assumption to hold, the length of their tissue had to be much greater than its diameter. As a result, they engineered tissues up

to 10 mm in length. This is over 3x as large as the cardiac microtissues engineered in current human cardiac fibrosis on-chip platforms. A limitation to these tissue lengths is cost of human cardiomyocytes and reagents, and making high throughput use of the platform an expensive task. Additionally, their method of deflecting the tissue with a flexible probe is a contact method of measuring stiffness which may perturb cells during the experiments and would be an issue that would want to be avoided.

Finally, the fabrication process of our platform is simple compared to other platforms described, and can be done using standard machine shop equipment (milling machine and laser cutter). It does not require complex chemistry to bond hydrogels to membranes as in *Liu et al.'s* platform, nor does it require knowledge of nonstandard equipment such as ultrasound transducers as in *Zareei et al.'s* ultrasound on-a-chip platform.

4.4 Addressing potential microtears in the tissue

In Section 3.2.2 it was stated that microtissues that displayed visible signs of tearing when stretched were not used as part of the experiment. However, the issue of microtears in the tissue which cannot be visibly seen still remains. When stretched, the stresses in the tissue at the site of a microtear is greater than the rest of the tissue. As a result, this portion of the tissue would experience increased strain. This would lead to inaccurate force measurements when measuring rod deflection, and thus would lead to an inaccurate measurement of the bulk tissue stiffness. One solution would be optically tracking regions of the tissue with digital image correlation. By analyzing the strain in different regions of the tissue post-experiment, it can be determined if a certain region was experiencing an increased amount of local strain, signaling the presence of potential microtears. These tissues that display non-uniform strain distributions can then be flagged and not used as part of the experimental data set, or, the strain from a different region can be used as the bulk strain of the tissue.

4.5 Addressing the lack of physiological conditions on the platform

The potential for this platform to be used as part of a cardiac fibrosis on-chip platform that can fully capture the microenvironment of a fibrotic myocardium and measure functional markers of fibrosis non-invasively depends on this platform being able to measure stiffness of physiologically relevant cardiac microtissues. For proof of concept, in this study, microtissues composed of just cardiac fibroblasts were used. However, cardiac microtissues used in *Wang et al.'s* and *Mastikhina et al.'s* platform are composed of fibroblast and cardiomyocytes. Realizing the full physiology of cardiac tissue lends itself to factors not first considered with simpler models. With the addition of cardiomyocytes, the length-tension relationship of cardiac tissue must be considered. The length-tension relationship, shown by the Frank-Starling Law in the heart, represents the relationship between stroke volume and end diastolic volume [48]. As the heart fills with blood during its relaxed diastole phase, the strain on the muscle fibers increases sarcomere length, which raises myofibrils sensitivity to calcium, causing actin-myosin bridges to form, raising the tension in the tissue [49]. The force of contraction at diastole end is then governed by the force-sarcomere relationship. Using the actuation platform to stretch cardiac tissues composed of cardiomyocytes would result in an increase in cardiomyocyte sarcomere length, causing actin-myosin bridges to form. This would result in tissue active tension affecting the deflection of the PDMS rod as deflection would then be a function of inherent tissue stiffness along with active tension in the tissue.

While this may add complexity to measuring the stiffness of cardiac tissue on-chip, the platform is capable of accommodating the length-tension relationship, and may even be used to provide more info about the progression of fibrosis if the length-tension relationship is studied. As described within the thesis, the platform can be programmed to displace the neodymium magnet a prescribed amount and can hold tissue in a deformed position. Thus, a future experimental protocol could be as follows: **i**) Displace the magnet a prescribed amount (~8-10% of tissues length). **ii**) hold tissue at this strain and observe deflection of PDMS rod when cardiomyocytes contract. The PDMS rod deflection would be a function of active tension and intrinsic tissue stiffness. **iii**) apply

blebbistatin to the tissue to inhibit contraction. Blebbistatin is a specific inhibitor with high affinity for myosin II, which when inhibited, blocks active muscle contraction [50]. It was shown to take effect 100 seconds after application in mouse intact cardiomyocytes [50], and cardiac tissues exposed to it recovered 90% of their action potential duration [15], thus showing promise for use in daily stiffness measurements of cardiac microtissues without fear of tissue damage. The PDMS rod deflection after application of blebbistatin would then be a function of intrinsic tissue stiffness only. **iv**) Repeat the experiment daily to observe changes in active tension and tissue stiffness. *Wang et al.* observed decreased contractile force in their Biowire model of fibrosis due to diminished Ca^{2+} handling [5]. Their platform however, kept tissues statically cultured, suspended around two polymer rods. Application of our platform with a physiologically relevant microtissue could perhaps explore this further, by seeing how stretch at time of measurement would affect the contractile force and Ca^{2+} handling.

Another limitation in this study was the assumption of linear elasticity. The quasi-static loading assumption used in this study fails to consider the viscous behavior cardiac tissue would experience in an *in vivo* environment. Movement towards a more physiologically relevant loading protocol will be necessary for the best depiction of myocardial stiffness. This becomes evident when examining the behavior of collagen in the extracellular matrix. In low strain and strain rate loading, collagen fibers are randomly oriented. As strain and strain rate increase, the collagen fibers become aligned in the direction of loading, causing an increase in the modulus of the tissue [44].

4.6 How to fix the actuation platform reliability issues

To gather data for this study, tissues were manually stretched on-chip to displace the metal rod, similar to how a stepper motor/neodymium magnet setup would displace the metal rod non-invasively. The actuation platform designed to non-invasively stretch tissues on-chip to measure their stiffness had reliability and sensitivity issues related to the magnetic coupling of the neodymium magnet to the metal rod on chip, and to the attachment of the tissue to the metal rod.

It is important to note that changes to the overall chip design would want to be avoided. The current platform setup allows for tissue culture on a chip similar to current human cardiac fibrosis on-chip platforms. The separate, non-contact actuation platform allows tissue culture to remain relatively unchanged. Design modifications that introduce external parts into the actual chip itself to translate the rod would pose additional design issues related to culture sterility. Thus, the suggestions for platform modification described below are related to fixing the issues with the actuation platform and not changes into the overall chip design.

The issue of magnetic coupling between the metal rod and neodymium magnet did not arise when testing the platform using rubber bands. When testing the platform using rubber bands, the rubber bands were tied around the metal rod and secured by curing a small amount of PDMS on the knot. Thus, the metal rod was unable to tear away from the rubber band if there was not a perfect coupling to the neodymium magnet or if the rod did not perfectly translate on the chip due to imperfections on the machined surface. When attempting to stretch the tissues using the actuation platform, any misalignment when handing the chip near the neodymium magnet would cause the metal rod to rotate/move quickly out of position and rip from the tissue. Aligning might have been an issue as lining the Petri dish in the correct orientation on the platform was not precise. The strength of the neodymium magnet meant that any degree of misalignment would create a strong magnetic force pulling on the small metal rod. The strength of the neodymium magnet also caused sudden metal rod movement if the rod got caught on an imperfection on the machined surface of the chip. If caught on an imperfection, a displacement gap between the magnet and metal rod would be created, as the stepper motor would continue to move the magnet according to protocol while the rod would be stuck. When the gap became large enough and the rod became unstuck, the resulting quick movement of the rod back to the magnet would cause the rod to rip from the tissue. Fabricating a Petri dish holder with one possible orientation to place the dish into could solve the unbalanced magnetic forces when placing the dish on the platform. To go with the new holder, a custom Petri dish could also be designed for testing purposes only.

When it is time to stretch the tissue, you could move it from the general Petri dish to the one with the geometry that lets in fit in the holder in only one possible orientation. Additionally, nylon runners could be fabricated onto the surface of the slot portion of the chip. This would allow a near frictionless movement path for the metal rod to translate, ensuring a reliable couple to the neodymium magnet.

The issue of attachment of the tissue to the metal rod is one which would need to be further investigated as well. A majority of the tissues showed weak attachment to the metal rod and would tear away when stretched by the neodymium magnet. It was thought that the weak attachment of the tissue to the metal rod was due to either the metal rod's stiffness, possible surface oxidation reactions, or just overall poor attachment to metal. AFM measurements were performed along the length of three tissues and only one tissue showed an increased stiffness at the metal rod end, suggesting the rod stiffness was creating a locally stiff tissue. If the greater stiffness of the metal rod is not the issue with tissue attachment, then potential oxidative reactions or poor contact near the metal end could be mitigated by coating the metal rods in a thin layer of PDMS as tissues attached well to the PDMS bar.

Chapter 5

5.0 Conclusion

In conclusion, we have developed a microtissue platform with integrated on-chip stiffness measurement capabilities. The platform was verified by comparing moduli of rubber bands measured on-chip to moduli of rubber bands measured using a tensile tester. No difference in modulus was found between the two methods, thus displaying an initial proof of concept for the platform. To demonstrate the stiffness measurement principles of the platform with live tissues, modulus measurements of cardiac microtissues were obtained by manually displacing the tissues on-chip and comparing to modulus measurements obtained using AFM. No difference in modulus was found between on-chip measurements and measurements made using AFM, showing that when the reliability issues plaguing this platform are resolved, full realization of a platform to non-invasively measure the stiffness of cardiac microtissues will be achieved. In the end, a platform capable of monitoring the stiffness of fibrotic cardiac microtissues throughout the duration of an experiment will be the next step in helping to uncover the mechanisms behind cardiac fibrosis.

Future steps for the platform involve improving the reliability issues with the magnet actuation platform. Currently, tissues are destroyed/unable to be measured as their attachment to the metal bar is not secure enough to withstand the variable forces the metal bar experiences in the neodymium magnets magnetic field. Additionally, moving towards a more relevant stretch protocol is necessary when measuring stiffness. The current protocol utilizes slow strain rates in order to approximate the tissue as a linear elastic solid. The actuation platform is capable of being programmed to initiate higher strain rates which would be helpful in measuring the full viscoelastic behavior of the cardiac tissue. Movement away from the liner elastic approximation would also require a new mathematical model for calculating stiffness as Hooke's Law only models the elastic behavior of a material.

6.0 References

[1] Braunwald E. *Heart Failure*. JACC: Heart Failure. 2013. **1(1)**: 1-20

[2] Hinz B., et al. *The myofibroblast: one function, multiple origins.* American Journal of Pathology. 2007. **170:** 1807-1816

[3] Kong M., et al. *Cardiac fibrotic remodeling on a chip with dynamical mechanical stimulation.* Advance Healthcare Materials. 2019. **8(3)**: 1801146

[4] Mastikhina O., et al. *Human cardiac-fibrosis-on-a-chip model recapitulates disease hallmarks and can serve as a platform for drug screening.* Biomaterials. 2020. **233.** 119741

[5] Wang E., et al. *Biowire Model of Interstitial and Focal Cardiac Fibrosis*. ACS Central Science. 2019; **5** (7): 1146-1158

[6] van Spreeuwel A., et al. *Mimicking cardiac fibrosis in a dish: Fibroblast density rather than collagen density weakens cardiomyocyte function*. Journal of Cardiovascular Translational Research. 2017. **10:** 116-127.

[7] Spencer T., et al. *Fibroblasts slow conduction velocity in a reconstituted tissue model of fibrotic cardiomyopathy.* ACS Biomaterials Science & Engineering. 2017. **3:** 3022-3028.

[8] Rohr S., et al. *Myofibroblasts in diseased hearts: new players in cardiac arrhythmias?* Heart Rhythm. 2009. **6:** 848-856.

[9] Sadeghi A., et al. *Engineering 3D cardiac fibrotic tissue to study fibrotic remodeling.* Advance Healthcare Materials. 2017. **6:** 1601344.

[10] Zhao H., et al. *Microengineered in vitro model of cardiac fibrosis through modulating myofibroblast mechanotransduction.* Biofabrication. 2014. **6:** 04009.

[11] Dobaczewski M., et al. *The extracellular matrix as a modulator of the inflammatory and reparative response following myocardial infarction.* Journal of Molecular and Cellular Cardiology. 2010. **48:** 504-511

[12] Frangogiannis N. *The immune system and cardiac repair.* Pharmacological Research. 2008. **58:** 88-111

[13] Siwik DA., et al. *Interleukin-1beta and tumor necrosis factor alpha decrease collagen synthesis and increase matrix metalloproteinase activity in cardiac fibroblast in vitro.* Circulation Research. 2000. **86:** 1259-1265

[14] Serini G., et al. *The fibronectin domain ED-A is crucial for myofibroblastic phenotype induction by transforming growth factor-beta1*. Journal of Cellular Biology. 1998. **142:** 873-881

[15] King. N., et al. *Mouse intact cardiac myocyte mechanics: cross-bridge and titin-based stress in unactivated cells.* The Journal of General Physiology. 2010. **137:** 81-90

[16] Factor S., et al. *Alterations of the myocardial skeletal framework in acute myocardial infarction with and without ventricular rupture.* American Journal of Cardiovascular Pathology. 1986. **1:** 91-97

[17] Janicki JS., & Brower G. *The role of myocardial fibrillar collagen in ventricular remodeling and function.* Journal of Cardiology Failure. 2002. **8:** 319-325

[18] Vasquez C., et al. *The origin and arrhythmogenic potential of fibroblasts in cardiac disease.* Journal of Cardiovascular Translational Research. 2012. **5 (6):** 760-767

[19] Annes J., et al. *Making sense of latent TGF-*β *activation.* Journal of Cell Science. 2003. **116:** 217-224

[20] Kong P., et al. *The pathogenesis of cardiac fibrosis*. Cell Mol. Life Sci. 2014. **71: 549-574**

[21] Hinz B. *Formation and function of the myofibroblast during tissue repair.* Journal of Investigative Dermatology. 2007. **127 (3)** 526-537

[22] Goffin J., et al. *Focal adhesion size controls tension-dependent recruitment of* α*-smooth muscle action to stress fibers.* The Journal of Cell Biology. 2006. **172 (2):** 259-268

[23] Heling A., et al. *Increased expression of cytoskeletal, linkage, and extracellular proteins in failing human myocardium.* Circulation Research. 2000.**86:** 846-853

[24] Zile M., & Brutsaert D. *New concepts in diastolic dysfunction and diastolic heart failure: Part I.* Circulation. 2002.**105:** 1387-1393

[25] Segura A., et al. *Fibrosis and heart failure.* Heart Failure Reviews. 2014. **19:** 173-185

[26] de Jong S., et al. *Fibrosis and cardiac arrhythmias.* Journal of Cardiovascular Pharmacology. 2011. **57:** 630-638

[27] Patten R., & Hall-Porter M. *Small Animal Models Of The Heart: Development of Novel Therapies, Past and Present.* Circulation: Heart Failure. 2009, **2** (2): 138-144

[28] Leist M., & Hartung T. *Inflammatory findings on species extrapolations: humans are definitely no 70-kg mice.*Archives of Toxicology. 2013*,* **87:** 563-567.

[29] Ferri, N., et al. *Drug attrition during pre-clinical and clinical development: understanding and managing drug-induced cardiotoxicity*. Pharmacol Ther. 2013, **138** (3): 470-84.

[30] Bhatia S.N., & Ingber D. *Microfluidic organs-on-chips.* Nature Biotechnology. 2014. **32 (8):** 760-772.

[31] Pontes Soares C., et al. *2D and 3D-Organized cardiac cells shows differences in cellular morphology, adhesion junctions, presence of myofibrils, and protein expression.* PLoS One. 2012. **7 (5):** e38147.

[32] Fung Y.C. *Structure and stress-strain relationship of soft tissue.* American Zoology. 1984. **24:** 13-22

[33] Liu H., et al. *Microdevice arrays with strain sensors for 3D mechanical stimulation and monitoring of engineered tissues*. Biomaterials. 2018. **172**: 30-40.

[34] Alhudaithy S., et al. *Design, fabrication, and validation of a petri dish-compatible PDMS bioreactor for the tensile stimulation and characterization of microtissues.* Micromachines. 2020. **11**: 892.

[35] Zareei A., et al. *A lab-on-chip ultrasonic platform for real-time and nondestructive assessment of extracellular matrix stiffness.* Lab on a Chip. 2020. **20:** 78.

[36] Sidorov V., et al. *I-Wire heart-on-a-chip I: Three-dimensional cardiac tissue constructs for physiology and pharmacology.* Acta Biomaterialia. 2017. **48:** 68-78.

[37] Hermida N., et al. *A synthetic peptide from transforming growth factor-b1type III receptor prevents myocardial fibrosis in spontaneously hypertensive rats*.Cardiovascular Research. 2009. **81** (3): 601-609

[38] Tan SM., et al. *Targeted inhibition of activin receptor-like kinase 5 signaling attenuates cardiac dysfunction following myocardial infarction*. Am J Physiol Heart Circ Physiol. 2010. **298** (5) :H1415–25

[39] Greek, R., Menache, A. *Systematic Reviews of Animal Models: Methodology vs. Epistemology.* International Journal of Medical Sciences. 2013. **10**: 206-221

[40] Fan Z., Guan J. *Antifibrotic therapies to control cardiac fibrosis*. Biomaterials Research. 2016. **20**

[41] Cheng Y.M. *Limitations to the large strain theory.* International Journal For Numerical Methods In Engineering. 1992; **33.** 101-114

[42] Ugural A., & Fenster S. *Advanced mechanics of materials and applied elasticity.* Prentice Hall. 2015. **5:** 71

[43] Stroud J., et al. *Viscoelastic properties of pressure overload hypertrophied myocardium: effect of serine protease treatment.* Am. J. Phy. Heart Circ. Physio. 2001. **282:** H2324-H2335

[44] Herchenhan A., et al. *Tenocyte contraction induces crimp formation in tendon-like tissue.* Model. Mechano. 2012. **11:** 449-459

[45] Tomasek J., et al. *Myofibroblasts and mechanoregulation of connective tissue remodeling*. Nature Reviews Molecular Cell Biology. 2002. **3:** 349-363.

[46] Liu H., et al. *A microfabricated platform with hydrogel arrays for 3D mechanical stimulation of cells.* Acta Biomaterialia. 2016. **34:** 113-124.

[47] Arts T., et al. *A model of the mechanics of the left ventricle.* Annals of Biomedical Engineering. 1979. **7:** 299-318

[48] Katz M. *Ernest Henry Starling, his predecessors, and the "law of the heart".* Circulation. 2002. **106 (23)**: 2986-2992.

[49] Kobirumaki-Shimozawa F., et al. *Cardiac thin filament regulation and the Frank-Starling mechanism.* The Journal of Physiological Science. 2014. **64 (4):** 221-232

[50] Kovacs M., et al. *Mechanism of blebbistatin inhibition of myosin II.* The Journal of Biological Chemistry. 2004. **279 (34):** 35557-35563

Appendix

Appendix A – Arduino Uno Code

```
// Connections to A4988
const int dirPin = 2;  // Direction
const int stepPin = 3; // Step

// Motor steps per rotation
const int STEPS_PER_REV = 10  //stepper motor moves 10 steps
;

void setup() {

  // Setup the pins as Outputs
  pinMode(stepPin,OUTPUT);
  pinMode(dirPin,OUTPUT);
}
void loop() {

  // Set motor direction clockwise
  digitalWrite(dirPin,LOW);

  // Move stepper motor
  for(int x = 0; x < (STEPS_PER_REV); x++) {
    digitalWrite(stepPin,HIGH);
    delayMicroseconds(500);    //0.5 seconds to send pulse to driver
    digitalWrite(stepPin,LOW);
    delayMicroseconds(500); //0.5 seconds for driver to move stepper motor
  }

  delay(2000); //wait 2 seconds

  // Set motor direction counterclockwise
  digitalWrite(dirPin,HIGH);

  // Move stepper motor
  for(int x = 0; x < (STEPS_PER_REV); x++) {
    digitalWrite(stepPin,HIGH);
    delayMicroseconds(500);
    digitalWrite(stepPin,LOW);
    delayMicroseconds(500);
  }

delay (2000); //wait 2 seconds
}
```

Appendix B – Figure Permissions

ELSEVIER LICENSE
TERMS AND CONDITIONS

Jan 15, 2021

This Agreement between Christian Paniccia ("You") and Elsevier ("Elsevier") consists of your license details and the terms and conditions provided by Elsevier and Copyright Clearance Center.

License Number	4982441071717
License date	Jan 05, 2021
Licensed Content Publisher	Elsevier
Licensed Content Publication	Biomaterials
Licensed Content Title	Human cardiac fibrosis-on-a-chip model recapitulates disease hallmarks and can serve as a platform for drug testing
Licensed Content Author	Olya Mastikhina,Byeong-Ui Moon,Kenneth Williams,Rupal Hatkar,Dakota Gustafson,Omar Mourad,Xuetao Sun,Margaret Koo,Alan Y.L. Lam,Yu Sun,Jason E. Fish,Edmond W.K. Young,Sara S. Nunes
Licensed Content Date	Mar 1, 2020
Licensed Content Volume	233
Licensed Content Issue	n/a
Licensed Content Pages	1
Start Page	119741
End Page	0
Type of Use	reuse in a thesis/dissertation
Portion	figures/tables/illustrations
Number of figures/tables/illustrations	1
Format	electronic
Are you the author of this Elsevier article?	No
Will you be translating?	No
Title	A Cardiac Tissue Platform with Integrated On-Chip Stiffness Measurement Capabilities
Institution name	University of Toronto
Expected presentation date	Jan 2021

ELSEVIER LICENSE
TERMS AND CONDITIONS

Jan 15, 2021

This Agreement between Christian Paniccia ("You") and Elsevier ("Elsevier") consists of your license details and the terms and conditions provided by Elsevier and Copyright Clearance Center.

License Number	4981211216483
License date	Jan 03, 2021
Licensed Content Publisher	Elsevier
Licensed Content Publication	Acta Biomaterialia
Licensed Content Title	I-Wire Heart-on-a-Chip I: Three-dimensional cardiac tissue constructs for physiology and pharmacology
Licensed Content Author	Veniamin Y. Sidorov,Philip C. Samson,Tatiana N. Sidorova,Jeffrey M. Davidson,Chee C. Lim,John P. Wikswo
Licensed Content Date	Jan 15, 2017
Licensed Content Volume	48
Licensed Content Issue	n/a
Licensed Content Pages	11
Start Page	68
End Page	78
Type of Use	reuse in a thesis/dissertation
Portion	figures/tables/illustrations
Number of figures/tables/illustrations	1
Format	electronic
Are you the author of this Elsevier article?	No
Will you be translating?	No
Title	A Cardiac Tissue Platform with Integrated On-Chip Stiffness Measurement Capabilities
Institution name	University of Toronto
Expected presentation date	Jan 2021
Portions	Figure 1